Mechanics of Materials 116 (2018) 104–119

Contents lists available at ScienceDirect

Mechanics of Materials

journal homepage: www.elsevier.com/locate/mechmat

Research paper

On the instability of chip flow in high-speed machining

G.G. Ye[b,*], M.Q. Jiang[a,c], S.F. Xue[b], W. Ma[d], L.H. Dai[a,c,*]

[a] State Key Laboratory of Nonlinear Mechanics, Institute of Mechanics, Chinese Academy of Sciences, Beijing 100190, China
[b] Department of Engineering Mechanics, College of Pipeline and Civil Engineering, China University of Petroleum, Shandong 266580, China
[c] School of Engineering Science, University of Chinese Academy of Sciences, Beijing 101408, China
[d] Key Laboratory of Environmental Mechanics, Institute of Mechanics, Chinese Academy of Sciences, Beijing 100190, China

ARTICLE INFO

Article history:
Received 29 October 2016
Revised 22 January 2017
Available online 1 March 2017

Keywords:
High-speed machining
Shear banding
Serrated chip flow
Thermoplastic instability

ABSTRACT

High cutting speed usually gives rise to a breakdown of steady chip flow and results in a serrated flow pattern, which is one of the most fundamental and challenging problems in metal cutting. Here, we systematically analysed the experimental results of high-speed cutting on various typical metallic materials over wide ranges of cutting speeds. With considering the coupling effects of inertial, tool-chip compression and material convection, the critical condition for the onset of serrated chip flow is determined based on a stability analysis of the deformation inside primary shear zone. It is found that the emergence of the serrated chip flow is dominated by a dimensionless number which characterized the competition among the effects of inertia, thermal softening, strain hardening, elastic unloading, viscous diffusion and thermal diffusion. More interestingly, a power law between the serration frequency and the *Reynolds* thermal number *Pe* is clearly revealed.

1. Introduction

Cutting is a ubiquitous activity in daily life, science and technology (Atkins, 2009; Dodd and Bai, 2012; Shaw, 2005). The metal cutting operation referred to as the chip formation process has been widely studied for its obvious economic and technical importance. Its roots go back at least 130 years to when Tresca (1878) presented pictures of viscoplasticity in metal cutting and Mallock (1881) drew sketches of chip formation. The growing demand for enhanced production efficiency and product quality has led to the rapid development of high-speed machining (HSM) technology. In spite of extensive studies, several fundamental aspects of the metal cutting process are poorly understood. One of these aspects is the onset of serrated chip flow. The puzzle of why continuously smooth chip flow in metal cutting gives way to periodically serrated chip flow as the cutting speed increases still remains elusive.

The formation of serrated chip flow has been extensively studied (Sutter and List, 2013; Vyas and Shaw, 1999). It is found that the emergence of serrated chip flow is usually related to shear banding occurring in the primary shear zone (PSZ), which is fuelled by a complex nonlinear coupling of high strain, high strain rate and high temperature rise during HSM (Recht, 1964; Ye et al., 2014). Because thermoplastic instability-induced shear banding is a major failure mechanism in impact loading (Bai and Dodd, 1992; Dodd and Bai, 2014), a fundamental understanding of the shear banding mechanism is of considerable interest to both the mechanics and the materials science communities. A large amount of excellent work regarding shear banding can be found in the literature (Aifantis, 1987; Daridon et al., 2004; Dodd et al., 2015; Grady, 1994; Meyers, 1994; Molinari, 1985; Nemat-Nasser and Okada, 2001; Rittel, 1998; Rittel and Wang, 2008; Walley, 2007; Zhang et al., 2005; Zhang et al., 2008).

The onset of thermoplastic instability-induced shear banding has been extensively examined, either through a maximum stress criterion, through linear stability analyses (Bai, 1982; Batra and Wei, 2006; Molinari, 1997), or through nonlinear analyses (Wright, 2002). How the shear band develops after instability and how it interacts with the boundaries or neighbouring localizations have also been extensively studied. The defining experimental results in shear localization were determined using a torsional Kolsky bar to generate shear bands within thin-walled tubes (Ramesh, 1994). By using a Kalthoff-type experiment, the initiation and propagation of shear bands in steel plates was examined by Zhou et al. (1996). The fully developed shear bands can be easily studied with collapsing cylinders (Xue et al., 2002). Batra and his co-workers (Batra, 1987; Batra and Kim, 1990) have performed some impressive research on the influences of material parameters and flow rules on both shear band initiation and growth. In the study of shear band interactions, Zhou et al. (2006b) analysed the interactions between a single shear band and its surroundings using a numerical

* Corresponding authors.
E-mail addresses: yegg@upc.edu.cn (G.G. Ye), lhdai@lnm.imech.ac.cn (L.H. Dai).

http://dx.doi.org/10.1016/j.mechmat.2017.02.006
0167-6636/

Nomenclature

English alphabet

V	cutting speed
b	uncut chip thickness
L	contact length between tool and chip
L_c	serration spacing
f	serration frequency
F	fb/V
f_{int}	friction stress along the tool surface
V_{chip}	material velocity along shear direction
V_s	tool velocity along shear direction
V_f	material convection velocity
Δu	compression displacement
c	work material specific heat
C	strain rate coefficient in J-C law
w	width of PSZ
n	work-hardening exponent in J-C law
E	work material elastic modulus
m	thermal softening coefficient in J-C law
Re	*Reynolds* number
k	wave number
$\bar{k}$	$\sqrt{\rho/Q_h}\lambda k$
Q_h	$(\partial\tau/\partial\gamma)_h$, strain hardening effect
R_h	$(\partial\tau/\partial\dot{\gamma})_h$, strain rate hardening effect
P_h	$-(\partial\tau/\partial\theta)_h$, thermal softening effect
C_L	$\sqrt{E/\rho}$, elastic wave velocity
C_{SP}	$\sqrt{Q_h/\rho}$, plastic shear wave velocity
C_λ	λ/b, thermal diffusion velocity
C_υ	$R_h/\rho b$, viscous diffusion velocity
Da	$\rho V^2\sin^2\varphi/Q_h$,effective damage number
Pr	C_υ/C_λ,*Prandtl* number
Pe	Vb/λ, *Péclect* number/thermal number
B	$\beta\tau_h P_h/\rho c Q_h$

Greek alphabet

ω	tool rake angle
φ	shear angle
σ	local compression stress
σ_x	normal stress along the x direction
ε	elastic compression strain
δ	scale of the local compression zone
τ	shear stress
γ	shear strain
$\dot{\gamma}$	shear strain rate
ρ	work material density
λ	work material thermal diffusion
μ	friction coefficient
β	Taylor–Quinney coefficient
θ	temperature
θ_o	room temperature in J-C law
θ_{melt}	melting temperature in J-C law
τ_A	initial yield stress in J-C law
τ_B	hardening modulus in J-C law
$\dot{\gamma}_{ref}$	reference strain rate in J-C law
υ	kinematic viscosity
α	Initial growth rate of perturbation
$\bar{\alpha}$	$\rho\lambda\alpha/Q_h$
Ω	b/w
ζ	$1+\mu\tan(\omega-\varphi)$
Γ	$2[1+\mu\tan(\omega-\varphi)]^{1/2}\sin\varphi$
Λ	$2\pi[4\cos(\omega-\varphi)/\Gamma^2\cos\omega]^{1/4}$
Φ	tool compression coefficient

Subscripts

h	homogeneous deformation solution
$*$	initial magnitude of perturbation

approach. Rittelet al. (2008; 2006) addressed adiabatic shear localization from a different point of view. They stated that the shear banding can be viewed as being triggered by dynamic recrystallization instead of being the result of thermal softening. In recent years, the formation and mechanism of shear banding have still received extensive attentions (Love and Batra, 2010; Osovski et al., 2013; Rodríguez-Martínez et al., 2015; Su and Stainier, 2015; Tvergaard, 2015; Yuan et al., 2015).

With regard to metal cutting, the shear band of the serrated chip almost forms inside the PSZ. So, considerable efforts have also been carried out to investigate the initiation of shear banding by analysing the flow stability of the PSZ, and several classical models have been developed to derive conditions under which the continuously smooth chip flow becomes unstable. The first explanation for the emergence of serrated chip flow was presented by Recht (1964), who stated that once the thermal softening effect of material in the PSZ overcomes the tendency to harden with plastic deformation, shear instability occurs. This model was later developed by Hou and Komanduri (1997) to predict the critical cutting speed for the onset of serrated chip flow. Semiatin and Rao (1983) provided another model for chip flow instability, in which a flow localization parameter is presented to judge whether serrated chip flow could take place. Later, by applying ideas from the theory of shear banding in torsion, Molinari and Dudzinski (1992) derived the conditions under which continuous chip flow becomes unstable. Burns and Davies (1997, 2002) explained the serrated chip flow as a bifurcation phenomenon. More recently, by considering the effect of the strain gradient, which becomes important in the case of shear banding, Aifantis and his co-workers (Huang and Aifantis, 1997; Huang et al., 2007) presented a method for thermo-viscoplastic instability in chip formation to describe the serrated chip flow. Childs (2013) predicted the onset of serrated chip flow using a thermal number or *Reynolds* thermal number *Pe*. Recently, Cai et al. (Cai et al., 2015; Cai and Dai, 2014) found that the serrated chip flow can be suppressed by imposing an extrusion constraint on the chip, and a theoretical model was developed to uncover the underlying mechanism. These pioneering works provide important clues to the study of the onset of serrated chip flow.

Most of the previous works studied the onset of serrated chip flow by modelling the PSZ as a simple shear. However, the deformation inside the PSZ is different with the simple shear, and the high speed makes the problem much more complex. The complexities of the high speed cutting can be characterized by the three following points:

1) First, the chip flow is very rapid at high cutting speed. The rapid chip flow takes material away from the PSZ, which gives rise to the material convection (Burns and Davies, 2002). The material convection removes heat and momentum from the PSZ and hence influences the plastic flow stability significantly.
2) Second, the shear deformation inside the PSZ is caused by the compression between chip and tool. The loading and unloading of the local compression of the chip affects the thermoplastic deformation behaviour in the PSZ.
3) Third, the high cutting speed results in a significant inertia effect though the PSZ is thin. Indeed, whether the inertia effect is significant or not depends upon the competition between the inertia time $t_{inertial}$ and the deformation time $t_{deformation}$ (Wu et al., 2003). The inertia and deformation time are defined as $t_{inertial}=\sqrt{\rho bw/\tau_A}$ and $t_{deformation}=1/(V_s/w)$ respectively, where ρ is work material density, b uncut chip thick-

Table 1
Chemical compositions.

Material	Component Wt. %													
IN 718	Ni	C	Cr	Si	Ti	Mn	Cu	S	Mo	Fe	Nb	Co	Al	B
	Bal	0.03	19.0	0.05	0.98	.003	0.02	.002	3.21	19.36	5.28	0.3	0.43	.003
Ti-6Al-4V	Ti	Al	V	Fe	N	H	O	C						
	Bal	5.99	4.2	0.2	.004	.005	0.1	0.01						
AISI 4340	Fe	C	Cr	Si	Ti	Mn	Cu	S	Mo	W	V	Ni	P	
	Bal	0.4	0.7	0.19	.003	0.56	0.12	.007	0.17	0.01	0.01	1.38	.008	
Al 7075	Al	Zn	Cr	Si	Ti	Mn	Cu	Mg	Fe					
	Bal	5.6	0.23	0.4	0.2	0.3	1.6	2.5	0.5					
C10200	Cu	O												
	Bal	<.001												

Table 2
Heat treatments.

Material	Heat treatments
IN 718	Annealed at 1253 K/1 hr, quick cool to 993 K, hold at 993 K/8 hr, cool to 893 K in furnace, hold at 893 K/8 hr, quick cool.
Ti-6Al-4V	Annealed at 973 K/2 hr, quick cool.
AISI 4340	No
Al 7075	Annealed at 775 K/3 hr, cool at 50 K per hour to 500 K, Solution treat under 900 K, aged at 250 K/8 hr.
C10200	No

ness, w width of PSZ, τ_A initial yield shear stress and V_s is the shear velocity of the cutting tool. If $t_{inertial}$ is comparable to or larger than $t_{deformation}$, the inertia effect should be considered; otherwise, it can be neglected (GDR MiDi, 2004). For low-speed cutting cases, the inertia effect is negligible because $t_{inertial} << t_{deformation}$ is usually satisfied. However, the inertia effect becomes significant in high speed cutting, because the inertial time could be close to or even larger than the deformation time at very high cutting speed. Take for example the high speed cutting of Ti-6Al-4V. In this case, $b = 100\,\mu m$, $w = 10\,\mu m$, $\rho = 4430\,kg\ m^{-3}$, $\tau_A = 452$ MPa, and the highest cutting speed $V = 60 m/s$. We found that $t_{inertial} \approx 10^{-7} s$ is very close to $t_{deformation} \approx 1.7 \times 10^{-7} s$. It shows clearly that, in high speed cutting, the inertia effect cannot be neglected.

These factors make the study of the onset of serrated chip flow much more difficult, the onset of serrated chip still remains one of the least understood manufacturing phenomena.

Moreover, after serrated flow occurs, the flow motion becomes periodic, and shear banding occurs repeatedly. The periodic shear banding leads to fluctuation of the cutting force and temperature. Thus its frequency, i.e., the serration frequency, is taken to be the most important parameter characterizing chip serration. A number of works have been carried out to investigate the changing tendency of serration frequency with cutting conditions (Calamaz et al., 2010; Molinari et al., 2002; Molinari et al., 2013; Yang et al., 2012). It should be noticed that the shear banding frequency is dominated by the loading rate for simple shear, in which the material is loaded all the time. As for HSM, the work material is shear loaded only when it stays inside the PSZ, and the loading time is controlled by the chip flow, which removes material from the PSZ. Thus, the shear banding frequency is dominated by the competition between the loading rate accelerating shear banding and the chip flow velocity hindering shear banding. Notice that increasing the cutting speed increases both the shear loading rate and the chip flow velocity. This results in a complex comprehensive effect on the shear banding frequency. The changing relation of serration frequency with cutting speed is still an open topic that requires further investigation.

In this work, HSM experimental results for five typical metal alloys were systematically analysed. It shows that upon increasing the cutting speed, the repeated localization into shear bands of plastic flow is responsible for the critical transition of chip flow from continuous to serrated. The stability analysis of the plastic deformation inside PSZ was carried out, where the coupling effects of inertial, tool-chip compression and material convection are considered. The critical condition for the onset of serrated chip flow is determined. Moreover, the frequency of the serrated chip flow is found to be followed a power-law dependence on the *Reynolds* thermal number *Pe*.

2. Experimental setup

In our previous work (Ye et al., 2014), we have carried out the high speed cutting experiments on five typical metal alloys, including Ti-6Al-4V,IN 718, AlSI 4340 steel, Al 7075 and copper (C10200). The chemical compositions and heat treatments for the five work materials are given in Table 1 and Table 2, respectively.

The high speed cutting experiments were performed by using a light-gas gun-based device (Ye et al., 2012), which is schematically presented in Fig. 1. The cutting tool is propelled by a light-gas gun in a launch tube, and two symmetrical work pieces are fixed at the exit of the tube. Orthogonal cutting occurs when the tool impacts the work pieces. The cutting conditions for Ti-6Al-4V, IN 718, AlSI 4340 steel, Al 7075 and C10200 are given in Table 3.

3. Experimental observation

The high speed cutting experiments for Al 7075, AISI 4340 steel, IN 718, and Ti-6Al-4V have shown that there exists a transition from continuously smooth flow to periodically serrated flow with increasing cutting speed, as shown in Fig. 2 (Ye et al., 2014).

At low cutting speeds, the chip is smooth, the deformation is homogeneous (see the magnified figure in Fig. 2b at $V = 0.05$ m/s), and the chip flow motion is steady. With increasing cutting speed, the chip flow becomes disturbed, the steady chip flow is broken by the periodic emergence of highly localized shear bands (as shown in Fig. 2b at $V = 4.07$ m/s), and the chip flow changes form continuous smooth to be periodically serrated. The experimental results show clearly that the repeated thermoplastic shear instability-induced shear banding is the primary reason for the observed serrated chip flow (Ye et al., 2014).

In this work, we further measured the serration frequency f at different cutting speeds for Al 7075, AISI 4340 steel, IN 718, and Ti-6Al-4V. We first measured the total spacing of 10 randomly selected adjacent serrations for each serrated chip and set the av-

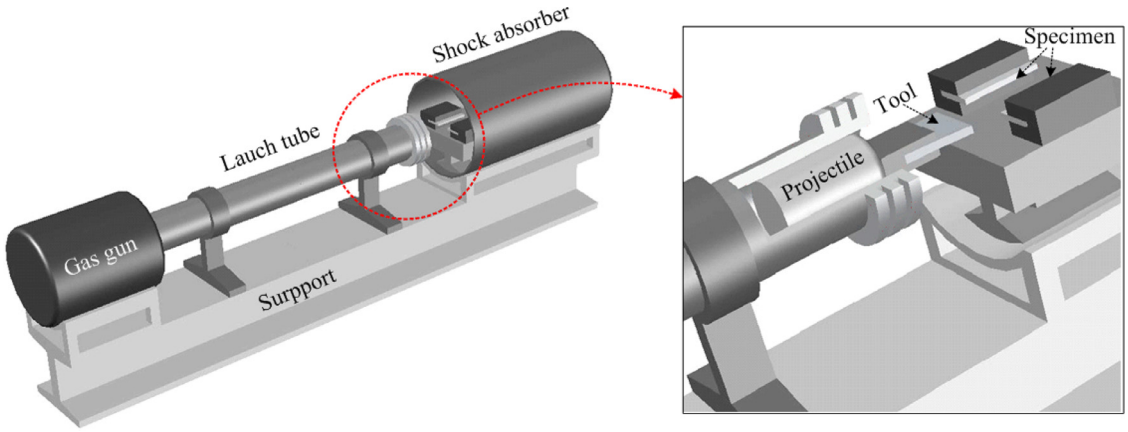

Fig. 1. Diagram of the light-gas-gun based cutting setup.

Table 3
Cutting parameters.

Material	Rake angle	Clearance angle	Uncut chip thickness	Cutting speed
IN 718	0°	7°	100 μm	0.05~36.7 m/s
Ti-6Al-4V	0°	7°	100 μm	0.05~60.5 m/s
AISI 4340	0°	7°	100 μm	2.0~32.4 m/s
Al 7075	0°	7°	100 μm	2.0~38.5 m/s
C10200	0°	7°	100 μm	2.0~89.9 m/s

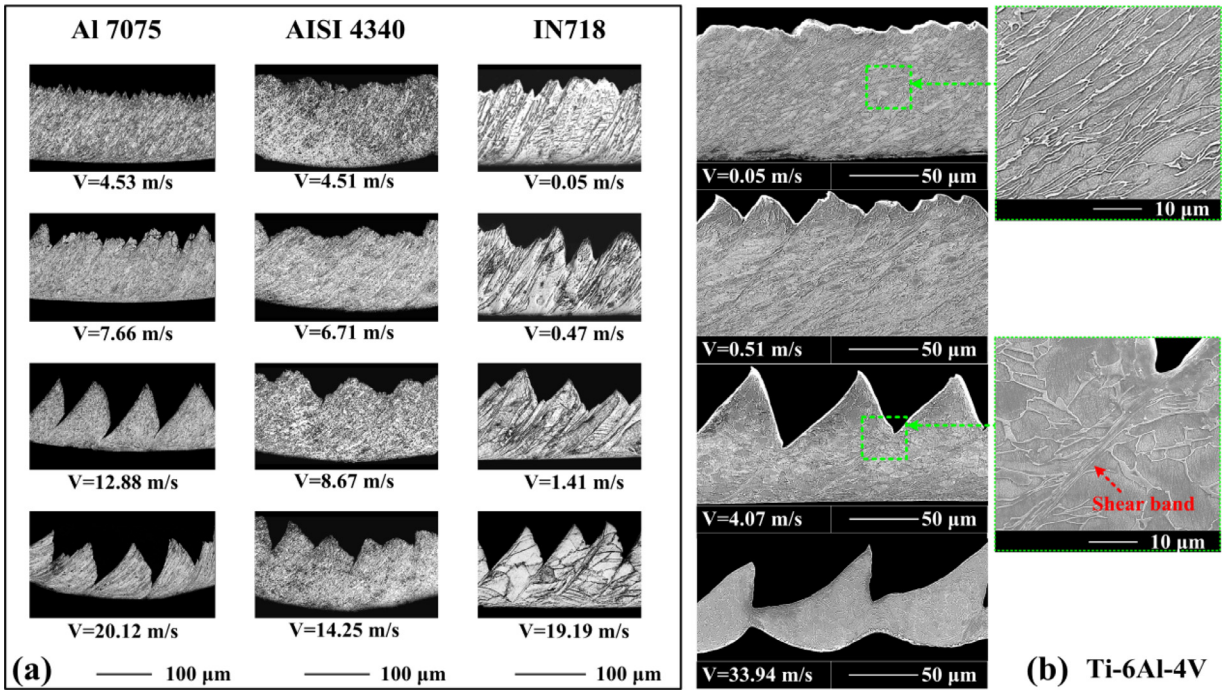

Fig. 2. Chip flow pattern evolves with cutting speed (a) for Al 7075, AISI 4340 steel, IN 718 (optical microscope images) and (b) for Ti-6Al-4V (scanning electron microscopy images).

erage spacing to be the serration spacing L_c, as shown in Fig. 3. Also, we measured the maximum thickness and minimum thickness of the serrated chip and set the average thickness to be the mean chip thickness b_c. By using $f = V\sin\varphi/L_c$ (Molinari et al., 2002), the serration frequency f can be determined. Here, the shear angle φ is estimated by the tool rake angle ω, the uncut chip thickness b and the measured mean chip thickness b_c according to $\sin\varphi/\cos(\omega+\varphi) = b/b_c$ (Vyas and Shaw, 1999). The serration spacing and frequencies for IN 718, Ti-6Al-4V, AISI 4340 steel and Al 7075 are given in Table 4.

It is interesting to find that the frequency of the periodically serrated flow pattern shows a power-law scaling with cutting speed; see Fig. 4. The serration frequency is plotted as a function of cutting speed on a double logarithmic scale for Ti-6Al-4V, IN 718, AISI 4340 and Al 7075. Four straight fitted lines ($\log(f) = \text{intercept} + 5/4 \times \log(V)$) with a slope of 5/4 are obtained, indicat-

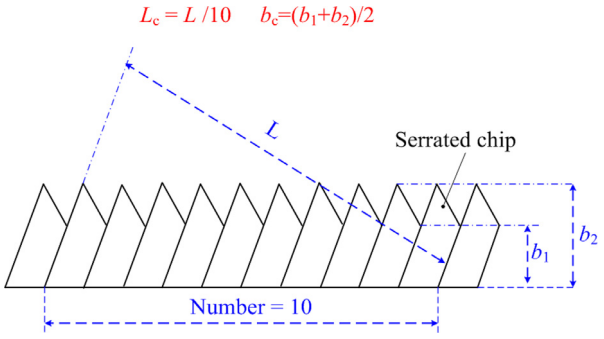

Fig. 3. Measuring of the serration spacing and the mean chip thickness.

ing a power-law dependence of serration frequency f on cutting speed V, $f \propto V^{5/4}$. The power-type relation between the serration frequency and the velocity is similar to the relation obtained between the fragment frequency and the expansion velocity in the ring expansion experiments (Grady and Olsen, 2003).

Moreover, we collected some other published experimental data(Asad et al., 2008; Atlati et al., 2011; Campbell et al., 2006; Cotterell and Byrne, 2008; Duan and Wang, 2004; Gao et al., 2011; Lorentzon et al., 2009; Lu and Xie, 2008; Mabrouki et al., 2008; Molinari et al., 2002; Pawade and Joshi, 2011; Sun et al., 2009; Sutter et al., 1997; Yang et al., 2012)and plotted them in log-log coordinate by cutting speed on the horizontal axis and serration frequency on the vertical, as shown in Fig. 5.

Figs. 5a∼**l** each correspond to a different work material (Ti-6Al-4V, IN 718, steels, Al 7075 and Al 2024) or a different cutting condition ($b = 50\sim400$ μm; $\omega = -10°\sim17.5°$; $V = 0.01\sim66$ m/s). It can be found that for different work material and different cutting condition, all the published data in each figure can be fitted by straight lines by with a universal slope of 5/4. This shows again that the serration frequency follows a power scaling law as a function of cutting speed according to $f \propto V^{5/4}$. Of course, the intercepts for the fitted lines are different because the material properties and cutting conditions are different.

4. Theoretical modelling

4.1. Thermo-mechanical coupling model

In this section, we develop a nonlinear thermo-mechanical coupling model to reveal the underlying physics of the flow mode transition and the scaling law for such serrated flow.

As has been discussed above, the transition from continuous chip flow to serrated chip flow can be attributed to the thermo-plastic shear instability which occurs during the continuous chip formation process. So, we first develop the thermo-mechanical coupling model for the continuous chip, and then, we investigate the initiation of serrated chip by analysing the flow stability of the work material inside the PSZ.

The cutting operation is referred to as the chip formation process. This process for the continuous chip is usually suggested to be one of concentrated shear along the PSZ extending upward from the tool point to the free surface (Shaw, 2005). The material is unstressed until it enters the PSZ. When it approaches this zone, stress builds up and plastic flow sets in. Subsequently, a chip separates from the original material and further flows along the tool face. This process is schematically presented by Fig. 6a. A Lagrangian coordinate system (x, y) is attached to the tool tip. Coordinates x and y are parallel and normal to the direction of shear flow, respectively. Here, the work material is assumed to be motionless and the tool to be moving with a constant cutting speed V.

The tool is in contact with chip over a length of L. The tool exerts a force on the chip over their contact surface, which makes the chip deform in a local compressive deformation zone. Here, the scale of the local compression zone is marked as δ, and the compression displacement along the shear direction is marked as Δu, as shown in Fig. 6a.

The tool-chip compressive stress induces a gradient in the shear stress, leading to a large scale shearing deformation that takes place in the PSZ. The shear angle is marked as φ. The stress condition of the PSZ is schematically presented in Fig. 6b. The material inside the PSZ is shear loaded along the x direction. It is also

Table 4
The measured average serration spacing and frequencies.

Material	Measured Results														
IN 718	V (m/s)	0.5	0.8	1.0	1.2	1.4	3.0	4.5	7.6	14.5	19.2	24.0	27.5	35.1	36.2
	L_c(μm)	69.1	76.5	78.0	66.6	69.0	60.0	52.1	44.0	42.3	40.4	34.2	28.8	30.7	35.3
	Standard deviation	13.4	12.8	12.7	10.6	10.8	10.1	8.6	8.1	7.8	7.6	7.1	6.8	6.2	6.5
	b_c(μm)	99.7	95.9	87.8	101.8	96.9	107.7	108.4	106.5	86.6	97.6	95.9	113.8	100.7	87.2
	φ(deg)	45.1	46.2	48.7	44.5	45.9	42.9	42.7	43.2	49.1	45.7	46.2	41.3	44.8	48.9
	f (kHz)	4.8	5.2	7.6	8.8	12.6	13.9	33.9	59.2	130.6	247.1	346.3	465.9	668.2	850.8
Ti-6Al-4V	V (m/s)	0.5	0.8	1.0	1.3	1.6	4.1	5.9	7.9	9.5	9.9	10.7	14.9	33.9	60.5
	L_c(μm)	45.2	64.3	52.1	57.9	54.8	52.3	49.7	47.8	50.5	49.3	43.3	37.2	37.9	31.1
	Standard deviation	12.2	13.1	12.1	11.7	10.9	10.6	10.8	10.1	9.3	9.5	8.7	8.2	7.4	5.9
	b_c(μm)	84.2	77.3	78.7	74.3	69.5	71.6	73.5	71.9	75.9	70.8	70.0	74.3	64.5	71.1
	φ(deg)	49.9	52.3	51.8	53.4	55.2	54.4	53.7	54.3	52.8	54.7	55.8	53.4	57.6	54.6
	f (kHz)	8.9	9.7	15.8	18.1	23.5	63.3	95.7	134.2	149.8	163.2	204.4	321.3	756.1	1587.5
AISI 4340	V (m/s)	6.7	8.7	10	14.3	18.0	19.1	24.2	28.0	31.9					
	L_c(μm)	70.2	70.4	61.8	55.3	58.4	57.1	47.9	45.8	50.3					
	Standard deviation	18.2	16.8	17.3	12.3	11.7	10.8	8.9	9.1	7.3					
	b_c(μm)	128.5	121.7	105.7	108.4	111.8	108.7	102.1	113.8	104.3					
	φ(deg)	37.9	39.4	43.2	42.7	41.8	42.6	44.4	41.3	43.8					
	f (kHz)	58.9	78.6	112.9	175.7	206.9	225.6	349.8	401.7	442.9					
Al 7075	V (m/s)	7.7	8.2	13.1	20.0	21.1	24.9	28.2	35.1	38.5					
	L_c(μm)	90.0	92.3	79.2	72.8	71.1	68.3	64.1	67.7	60.0					
	Standard deviation	16.7	16.2	14.5	13.2	12.8	12.7	11.6	9.8	9.3					
	b_c(μm)	109.1	91.6	88.8	76.2	78.7	73.7	83.0	75.9	74.3					
	φ(deg)	42.5	47.5	48.4	52.7	51.8	53.6	50.3	52.8	53.4					
	f (kHz)	57.5	65.4	121.9	217.9	232.4	295.9	336.6	409.9	515.1					

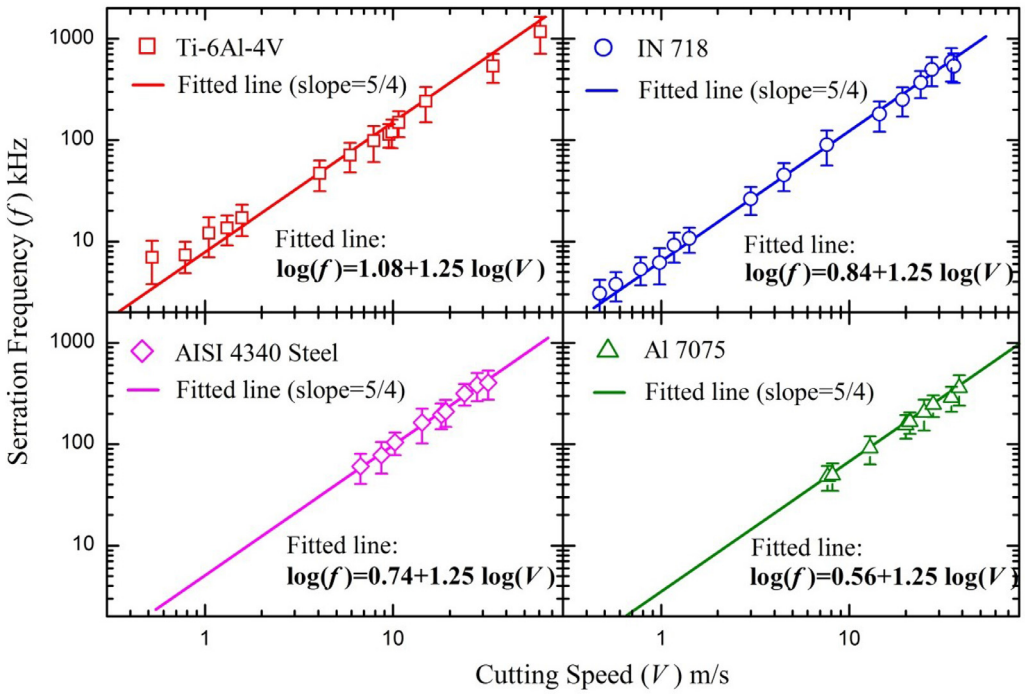

Fig. 4. Chip serration frequency versus cutting speed for Ti-6Al-4V, IN 718, AISI 4340 and Al 7075.

suffered by the compression and friction of the cutting tool. More importantly, the material inside the PSZ not only flows along the shear direction but also moves outwards from the PSZ with chip flow. This leads to material convection or mass transfer perpendicular to the shear direction, with a convection velocity marked as V_f.

In order to construct the thermo-mechanical coupling model for the continuous chip, the orthogonal cutting condition is assumed, and some other premises are made as follows:

i. The compressive deformation of the chip caused by the tool is small (Burns and Davies, 1997), so we assume the compressive deformation to be elastic.
ii. For simplicity, the scale of local compression zone δ is assumed to be same throughout the PSZ, from entry boundary *AB* to exit boundary *CD*. It is set to be approximately equal to the length of the PSZ, namely, $\delta = b/\sin\varphi$.
iii. The larger-scale shearing deformation inside PSZ can be is assumed to be rigid-thermoviscoplastic.
iv. The work material is assumed to be incompressible.

4.2. Governing equations

The deformation localized in the PSZ, which can be characterized by high temperature and strain rate, is the most important process for chip formation. Most previous works have been carried out to investigate the stability of the PSZ by treating it as a simple or adiabatic shear. However, as was noted in the introduction, material convection and chip-tool compression occur during high-speed cutting. They make the problem much more complex. Here, focusing on the PSZ and considering the effects of inertial, material convection and the dynamic loading/unloading of the tool-chip compression, we determine the basic equations governing the thermo-mechanical flow inside the PSZ:

(a) *Constitutive relation for plastic shear stress*

The larger-scale shearing deformation inside PSZ can is assumed to be rigid-thermoviscoplastic. Usually, the shear plastic flow is governed by the coupling effects of strain hardening, rate hardening and thermal softening. Hence, we use the constitutive model for shear plastic flow,

$$\tau = f(\gamma, \dot{\gamma}, \theta) \tag{1}$$

where τ is the shear stress, γ is the shear strain, $\dot{\gamma}$ is the shear strain rate, and θ is the temperature.

(b) *Loading/unloading equation of tool-chip compressive stress*

The tool exerts a force on the chip over their contact area, causing the chip to deform in a local compressive deformation zone. The compressive deformation of the chip is assumed to be elastic. Thus the compressive strain along the x direction can be approximately written as $\varepsilon_x = \Delta u/\delta$, where Δu is the compression displacement along the shear direction and δ is the scale of the local compression zone, as shown in Fig. 6a.

During the elastic compressive deformation, the local compressive stress along the x direction is proportional to the compressive strain and hence follows Hooke's law as:

$$\sigma = E\Delta u/\delta, \text{ before yielding} \tag{2}$$

where E is the elastic modulus.

It should be noticed that, Δu is caused by the difference between the velocity of the tool and the flow velocity of the work material in the direction of shear. Inside the PSZ, the material flow velocity along the shear direction is quite different from the entry boundary *AB* to the exit boundary *CD* (Oxley, 1989). And thus Δu should vary rapidly along the tool surface from *AB* to *CD*, see the detail of PSZ in Fig. 6b. This will result in a gradient of the local compression stress along the tool surface.

Differentiation the Eq. (2) with respect to the time t we can get that, the rate of change of the compressive stress is proportional to the difference between the tool velocity and the material flow velocity along the shear direction (x direction). Thus the loading process can be characterized by

$$\frac{d\sigma}{dt} = \frac{E}{\delta}\left(V_s - V_{chip}\right), \ before\ yielding \tag{3}$$

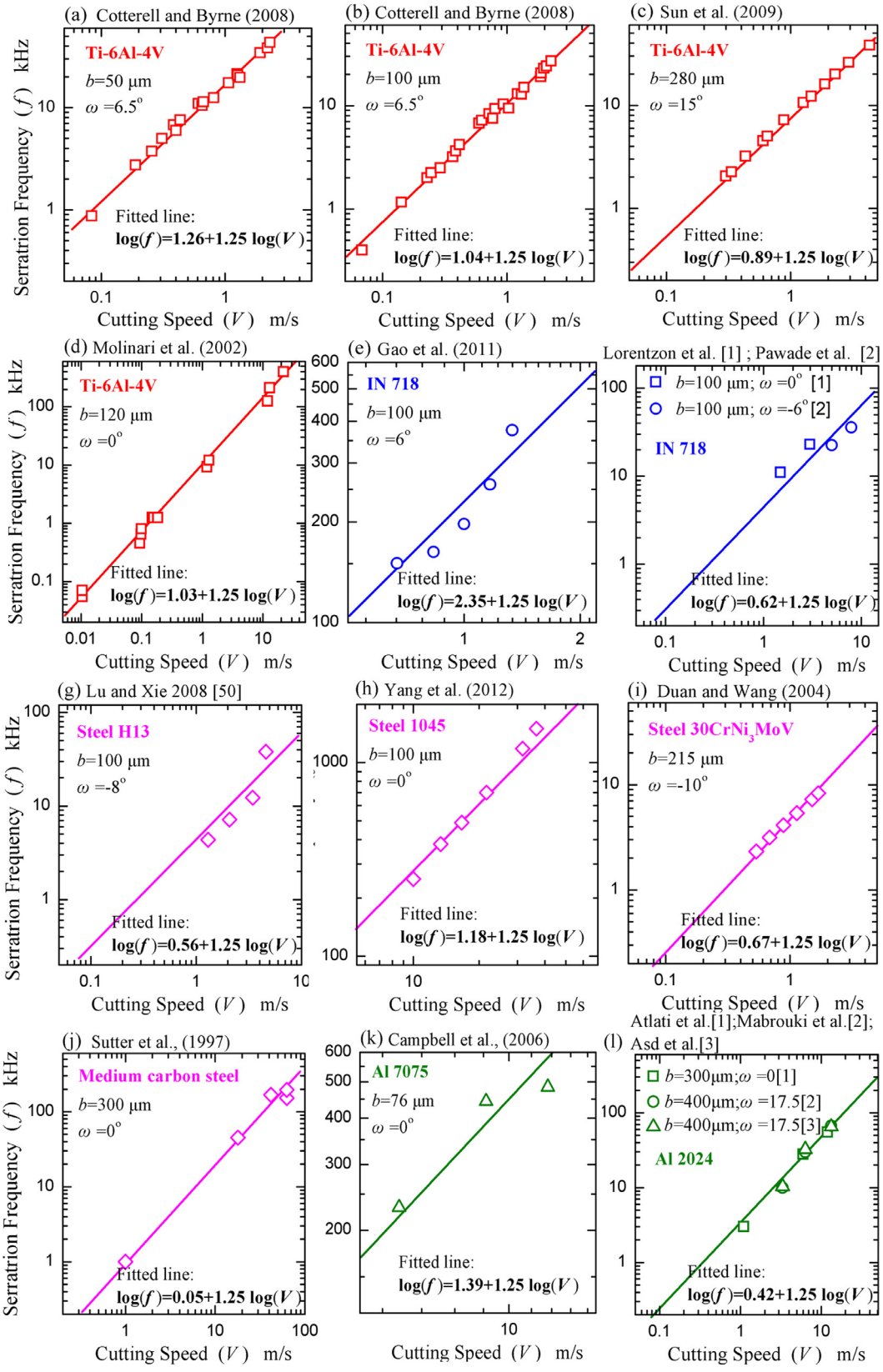

Fig. 5. f plotted with V for various materials under different cutting conditions.

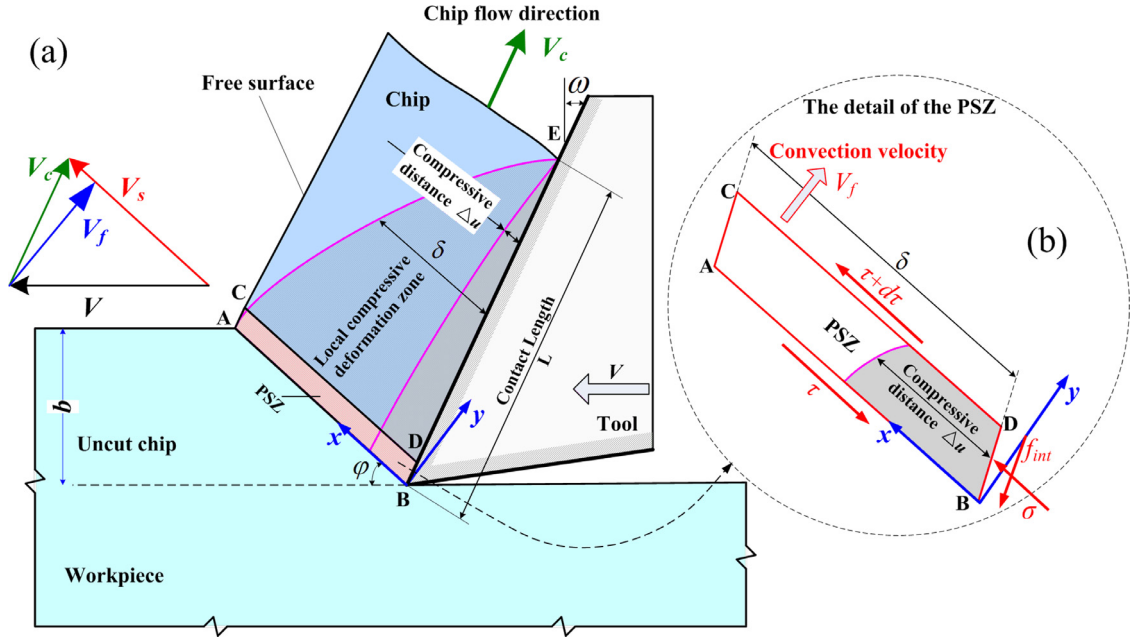

Fig. 6. Cutting model.

where $V_s = V\cos\omega/\cos(\varphi-\omega)$ is the tool velocity along the shear direction (x direction), and V_{chip} is the material velocity along the shear direction.

The compressive stress could increases locally before yielding. Here the Mises yield criterion is adopted. Inspired by the work of Burns and Davies (2002), we assume that the elastic unloading of local compression occurs after the PSZ stress condition reaches the yielding criterion:

$$\frac{d\sigma}{dt} = -\frac{E}{\delta}V_{chip},\ \ after\ yielding \tag{4}$$

During cutting, the material inside the PSZ not only flows along the shear direction but also moves along the tool surface with chip flow. This results in material convection perpendicular to the shear direction, with a convection velocity $V_f = V\sin\varphi$. Thus, $d()/dt$ can be further given by $\partial()/\partial t + V_f\partial()/\partial y$.

Noticing that the material velocity V_{chip} and the material shear strain rate $\dot{\gamma}$ satisfy the compatibility equation

$$\dot{\gamma} = \frac{\partial V_{chip}}{\partial y} = \frac{\partial\gamma}{\partial t} + V_f\frac{\partial\gamma}{\partial y} \tag{5}$$

This way, differentiating with respect to the ordinate y, both the loading Eq. (4) and the unloading Eq. (5) can be rewritten in a same way:

$$\frac{\partial^2\sigma}{\partial t\partial y} + V_f\frac{\partial^2\sigma}{\partial y^2} = -\frac{E}{\delta}\left(\frac{\partial\gamma}{\partial t} + V_f\frac{\partial\gamma}{\partial y}\right) \tag{6}$$

Eq. (6) characterizes the dynamic loading and unloading of tool-chip local compression.

(c) *Kinematic equation along x direction*

The stress condition of the PSZ is schematically presented in Fig. 6b.

The tool-chip interface BD is suffered by the local compression stress σ and friction stress f_{int}. And the boundary AC is regarded as a force free surface. As thus, the gradient of the normal stress along the x direction ($\partial\sigma_x/\partial x$) can be approximately given by

$$\frac{\partial\sigma_x}{\partial x} = \frac{\sigma + f_{\rm int}\sin(\omega-\varphi)}{|AB|} = \frac{\zeta\sin\varphi}{b}\sigma \tag{7}$$

where ζ is defined as $\zeta = 1+\mu\tan(\omega-\varphi)$, in which μ is the friction coefficient between the tool and chip.

As thus, the motion equation along the x direction can be implied as

$$\frac{\partial\tau}{\partial y} + \frac{\zeta\sin\varphi}{b}\sigma = \rho\frac{dV_{chip}}{dt} \tag{8}$$

where ρ is the work material density.

Differentiating Eq. (8) with respect to ordinate y and considering the material convection, we can get that

$$\frac{\partial^2\tau}{\partial y^2} + \frac{\zeta\sin\varphi}{b}\frac{\partial\sigma}{\partial y} = \rho\frac{d\dot{\gamma}}{dt} \tag{9}$$

where $d\dot{\gamma}/dt = \partial^2\gamma/\partial t^2 + 2V_f\partial^2\gamma/\partial t\partial y + V_f^2\partial^2\gamma/\partial y^2$.

It should be noted that the inertial effect denoted by $\rho(d\dot{\gamma}/dt)$ in Eq. (9) will become more significant with increasing cutting speed into the high-speed range. This is because the inertial time could be close to or even larger than the deformation time at high cutting speeds.

(d) *Energy equation*

The heat conduction is governed by Fourier's law, the energy equation in the PSZ can be given as

$$\frac{d\theta}{dt} = \frac{\beta\tau}{\rho c}\frac{d\gamma}{dt} + \lambda\frac{\partial^2\theta}{\partial y^2} \tag{10}$$

where c is work material thermal capacity, λ thermal diffusivity and β the Taylor–Quinney coefficient.

With considering the influence of material convection, the energy equation becomes

$$\frac{\partial\theta}{\partial t} = \frac{\beta\tau}{\rho c}\left(\frac{\partial\gamma}{\partial t} + V_f\frac{\partial\gamma}{\partial y}\right) + \lambda\frac{\partial^2\theta}{\partial y^2} - V_f\frac{\partial\theta}{\partial y} \tag{11}$$

Eq. (11) states that there are three different physical processes that can alter the PSZ temperature: heat generation because of plastic working (the first term) and diffusion and material convection (the second and third terms, respectively).

This way, the basic equations governing the deformation of the material inside PSZ can be listed as follows:

$$\tau = f(\gamma,\dot{\gamma},\theta) \tag{12a}$$

$$\frac{\partial^2\sigma}{\partial t\partial y}+V_f\frac{\partial^2\sigma}{\partial y^2}=-\frac{E}{\delta}\left(\frac{\partial\gamma}{\partial t}+V_f\frac{\partial\gamma}{\partial y}\right) \tag{12b}$$

$$\frac{\partial^2\tau}{\partial y^2}+\frac{\zeta\sin\varphi}{b}\frac{\partial\sigma}{\partial y}=\rho\left(\frac{\partial^2\gamma}{\partial t^2}+2V_f\frac{\partial^2\gamma}{\partial t\partial y}+V_f^2\frac{\partial^2\gamma}{\partial y^2}\right) \tag{12c}$$

$$\frac{\partial\theta}{\partial t}=\frac{\beta\tau}{\rho c}\left(\frac{\partial\gamma}{\partial t}+V_f\frac{\partial\gamma}{\partial y}\right)+\lambda\frac{\partial^2\theta}{\partial y^2}-V_f\frac{\partial\theta}{\partial y} \tag{12d}$$

where Eq. (12a) is the shear plastic flow model, Eq. (12b) is the loading/unloading equation of tool-chip compressive stress, Eq. (12c) is the motion equation along shear direction, and Eq. (12d) is the energy equation. These equations integrate the heat, stress and deformation of the cutting system in a coupled manner.

As stated in the introduction, the key differences between high speed cutting and simple shear is that material convection and tool-chip take place in high speed cutting, while not in simple shear. When the tool-chip compression and material convection are ignored, the problem is degenerated into the simple shear condition and the governing Eq. (12a)–(d) are reduced to

$$\tau=f(\gamma,\dot\gamma,\theta) \tag{13a}$$

$$\frac{\partial^2\tau}{\partial y^2}=\rho\frac{\partial^2\gamma}{\partial t^2} \tag{13b}$$

$$\frac{\partial\theta}{\partial t}=\frac{\beta\tau}{\rho c}\frac{\partial\gamma}{\partial t}+\lambda\frac{\partial^2\theta}{\partial y^2} \tag{13c}$$

For simple shear, Bai (1982) has obtained the instability criterion by using the linear perturbation analysis on the governing Eq. (13a)-(c) (Bai, 1982). As for HSM, the governing equations are more complex, thus the instability criterion should be different from that of the simple shear. In Section 5, we will achieve the onset condition of the serrated chip flow by study the stability of the PSZ deformation which governed by the Eq. (12a)-(d).

4.3. Homogeneous deformation

For continuous chip flow, the shear deformation inside PSZ is homogenous, which is a steady-state process. The shear banding formation in serrated chip flow is a result of the instability of homogeneous shear deformation for continuous chip flow. Therefore, we first examine the homogeneous shear deformation, which would provide some clues for understanding the resultant shear instability process.

According to Oxley (1989), during the homogeneous deformation for continuous chip flow, the shear strain rate can be assumed to be constant throughout the PSZ and to be given by

$$\dot\gamma=\frac{V_s}{w} \tag{14}$$

where $V_s=V\cos\omega/\cos(\varphi-\omega)$ is the tool shear velocity, w is the width of the PSZ which is usually set to be 1/10 of the uncut chip thickness (Burns and Davies, 2002). Therefore, for homogeneous shear deformation ($\partial\gamma/\partial y=\partial\dot\gamma/\partial y=0$), the original governing Eq. (12b)–(d) become

$$\frac{\partial\sigma}{\partial y}=-\int\frac{E\sin\varphi}{b}\dot\gamma\,dt \tag{15a}$$

$$\frac{\partial^2\tau}{\partial y^2}+\frac{\zeta\sin\varphi}{b}\frac{\partial\sigma}{\partial y}=0 \tag{15b}$$

$$\frac{\partial\theta}{\partial t}=\frac{\beta\tau}{\rho c}\dot\gamma+\lambda\frac{\partial^2\theta}{\partial y^2}-V_f\frac{\partial\theta}{\partial y} \tag{15c}$$

The initial conditions (IC) and the boundary conditions (BC) are given by

$$\text{IC}\begin{cases}V_{chip}(w,0)=V_s\\ \theta(y,0)=\theta_o\end{cases},\quad \text{BC}\begin{cases}V_{chip}(0,t)=0\\ \theta(0,t)=\theta_o\end{cases} \tag{16}$$

where θ_o is room temperature, which is set to be 300 K as a constant.

During homogeneous shear deformation, the inertial term in the kinematic equation vanishes naturally and the gradient of the shear stress should be balanced by the local compressive stress.

There are many constitutive laws can be used to describe the coupling effects of strain hardening, rate-hardening and thermal softening (Nemat-Nasser and Guo, 2003, 2005; Nemat-Nasser et al., 2001). Here, the widely used Johnson–Cook (J-C) model is adopted:

$$\tau=\left(\tau_A+\tau_B\left(\frac{\gamma}{\sqrt{3}}\right)^n\right)\left[1+C\ln\left(\frac{\dot\gamma}{\dot\gamma_{ref}}\right)\right]\left[1-\left(\frac{\theta-\theta_o}{\theta_{melt}-\theta_o}\right)^m\right] \tag{17}$$

where τ_A is initial yield stress, τ_B hardening modulus, n work-hardening exponent, C strain rate dependency coefficient, m thermal softening coefficient, $\dot\gamma_{ref}$ reference strain rate, θ_o room temperature, and θ_{melt} melting temperature.

By integrating Eqs. (15a)-(c) and (17) at the centre of the PSZ subject to the initial and boundary conditions Eq. (16), the evolution of the shear strain rat, shear strain, shear stress and temperature with loading time can be obtained. As thus, the shear stress - shear strain and temperature - shear strain curves can be plotted, and the steady-state solutions of shear flow stress and temperature at any loading shear strain can be determined.

Here, we take the Ti-6Al-4V for example to show the evolutions of shear stress and temperature with shear strain under different cutting speeds. The mechanical properties and parameters for Ti-6Al-4Vis listed in Table 5 (Lee and Lin, 1998).

To examine the effects of tool-chip compression and material convection on thermo-plastic behaviour within the PSZ, here we discuss four typical cases: (i) adiabatic deformation, where the material convection and diffusion terms in Eq. (15c) vanish; (ii) conventional deformation, where the diffusion is considered and the material convection term in Eq. (15c) vanishes; (iii) convective deformation, where the diffusion and material convection are considered simultaneously; and (iv) coupling deformation, in which the tool-chip local compression is considered in addition to the material convection and diffusion. For deformations (i)-(iii), the tool-chip local compressive stress is neglected. For these three cases, the shear stress and temperature are also homogeneous throughout the PSZ, the heat flow is set to occur only on the boundary surfaces of the PSZ, and the convection and diffusion terms in Eq. (15c) are approximately estimated by $-2\lambda\theta/w^2$ and $V_f\theta/w$ (Ye et al., 2012), respectively. Here, the Taylor–Quinney coefficient β is set to be a constant, 0.9.

Fig. 7 shows the shear stress versus shear strain at different cutting speeds during homogeneous deformation for Ti-6Al-4V.

The coupling deformation (iv) could more closely reflect the actual thermo-plastic deformation inside PSZ before instability. For the Ti-6Al-4V, strain hardening occurs over the whole deformation process at lower cutting speed ($V<0.5$ m/s) for the coupling deformation, and the stress dropping occurs as the cutting speed increases to a critical cutting speed ($V>0.5$ m/s). There exists a continuing strain softening after the peak stress, resulting in shear banding. This shows good agreement with the experimental results.

For convective deformation (iii), plastic yielding occurs earlier and the peak stress is lower than the coupling one; see Fig. 7. Moreover, the plastic yielding occurs at a lower cut-

Table 5
Mechanical properties and parameters of Ti-6Al-4V.

E (GPa)	ρ (kg m^{-3})	λ (m^2 s^{-1})	c (J kg^{-1} K^{-1})	τ_A (MPa)	τ_B (MPa)	C	n	m	$\dot{\gamma}_{ref}$ (s^{-1})	θ_{melt} (K)
105	4430	3×10^{-6}	520	452	287	0.028	0.28	1	1.73×10^{-5}	1880

ting speed for the convective deformation (iii). These results imply that the activation energy softening the material for coupling deformation (iv) is higher than that for convective deformation (iii). Therefore, the tool-chip compression makes it more difficult for strain softening to occur, which stabilizes the PSZ deformation.

Similarly, by comparing the convective deformation (iii) with the adiabatic (i) and conventional deformation (ii), it can be seen that it is more difficult for the plastic yielding to occur in the case of convective deformation. This indicates that the material convection hinders the emergence of serrated chip flow. The material convection results from the rapid chip flow, which removes heat from the PSZ and restricts the temperature rise. This weakens the thermal softening inside the PSZ and hence retards the occurrence of plastic yielding.

Fig. 8 shows temperature inside PSZ versus shear strain at different cutting speeds during homogeneous deformation for Ti-6Al-4V.

For each cutting speed, the coupling deformation temperature is lower than the convective one, and the convective deformation temperature is lower than the adiabatic and the conventional ones. This implies that both tool-chip compression and material convection restrict the temperature rise, which weakens the thermal softening effect in the PSZ and hence retards the occurrence of stress dropping. This is in accordance with the tendency of the shear stress evolution.

5. Onset of serrated chip flow

5.1. Perturbation analysis

As a physically unstable event, serrated chip flow can be regarded as the appearance of a mathematical instability in the differential equations governing the inhomogeneous flow. Usually, the stability analysis is simplified by seeking an inhomogeneous deformation solution with respect to small perturbations on the steady-state solution. The small perturbation method has been widely used to solve the shear banding problem. Examples of this method can be found in the works of Bai (1982) and Bai and Dodd(1992).

Here, we impose a perturbation (τ',γ', θ', σ') on the steady-state solution (τ_h, γ_h, θ_h, σ_h) to the problem, such that

$$\tau=\tau_h+\tau';\ \ \gamma=\gamma_h+\gamma';\ \ \theta=\theta_h+\theta';\ \ \sigma=\sigma_h+\sigma' \tag{18}$$

The perturbation has the following form:

$$\begin{aligned}\tau' &= \tau_* e^{\alpha t+iky}\\ \gamma' &= \gamma_* e^{\alpha t+iky}\\ \theta' &= \theta_* e^{\alpha t+iky}\\ \sigma' &= \sigma_* e^{\alpha t+iky}\end{aligned} \tag{19}$$

where(τ_*,γ_*, θ_*, σ_*) are small constants characterizing the initial magnitude of the perturbation, k is the wave number, and α is the initial growth rate of the perturbation. If α has a root with a positive real part, it implies that instability is possible, and serrated chip flow will be imminent.

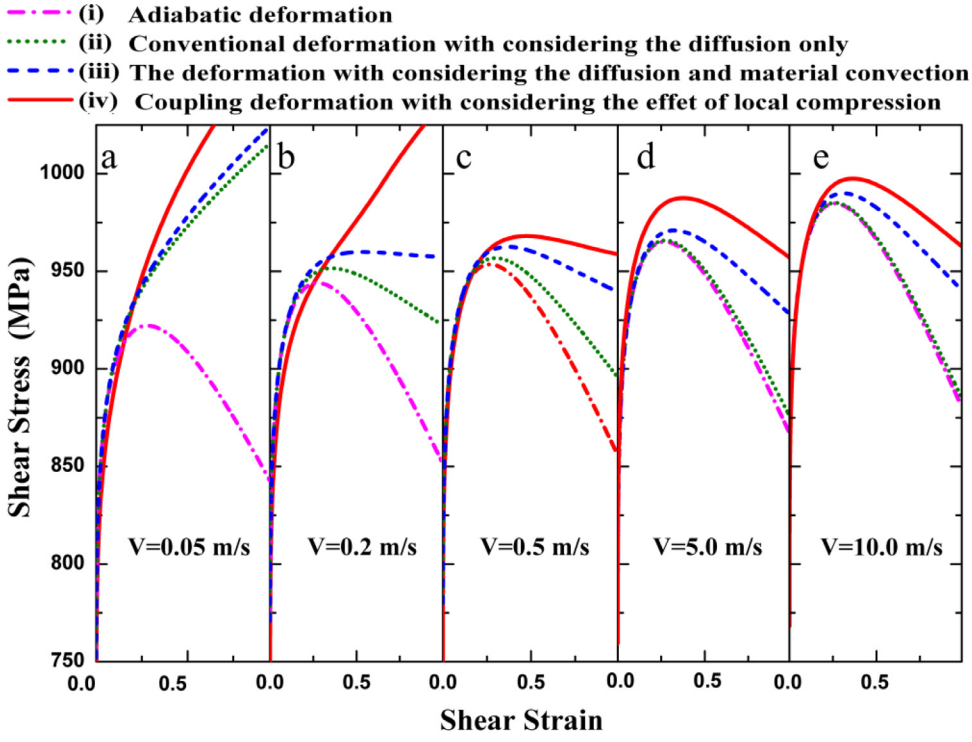

Fig. 7. Shear stress versus shear strain at different cutting speeds for Ti-6Al-4V.

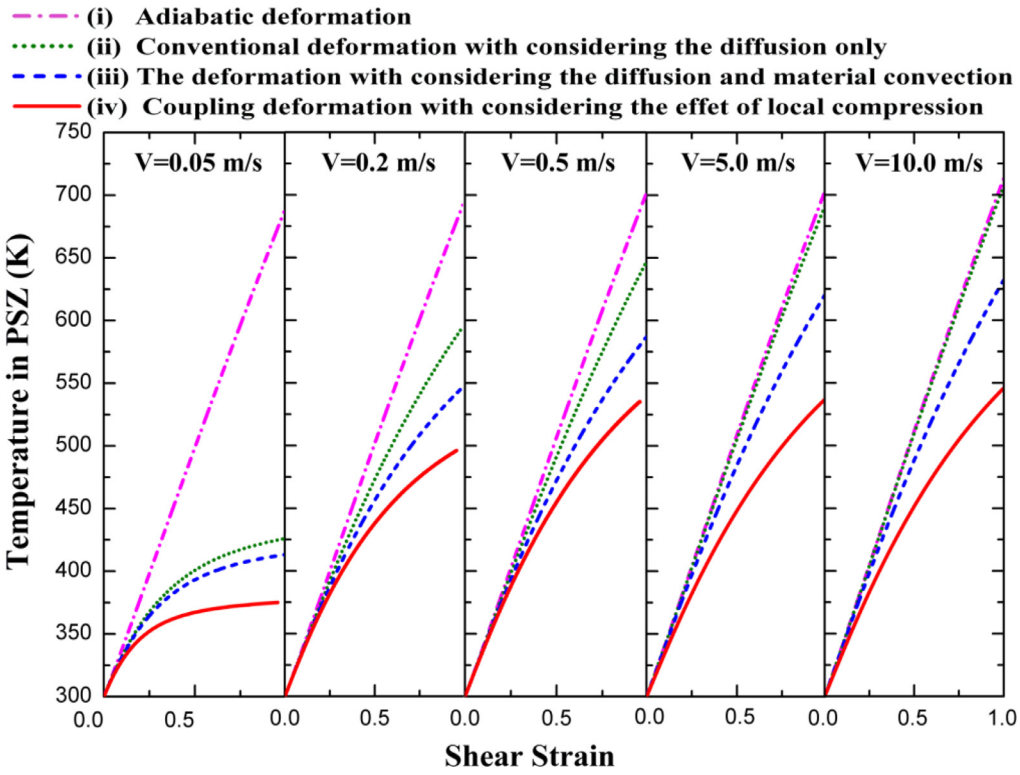

Fig. 8. PSZ Temperature versus shear strain at different cutting speeds for Ti-6Al-4V.

Introducing Eqs. (18) and (19) into the basic governing Eqs. (12a)–(d) and only considering terms that are of first order in $(\tau', \gamma', \theta', \sigma')$ leads to the spectral equation for the initial growth rate α of the perturbation:

$$\bar{\alpha}^3 + a_2\bar{\alpha}^2 + a_1\bar{\alpha} + a_0 + \left(3\bar{\alpha}^2 + b_1\bar{\alpha} + b_0\right)V\sin\varphi\sqrt{\rho/Q_h}\bar{k}i = 0 \tag{20}$$

where

$$a_2 = \beta\lambda P_h\dot{\gamma}_h/cQ_h + (1 + R_h/\rho\lambda)\bar{k}^2 \tag{21a}$$

$$a_1 = \left(1 + R_h\bar{k}^2/\rho\lambda - \beta\tau_h P_h/\rho cQ_h - 3\rho V^2\sin^2\varphi/Q_h\right)\bar{k}^2 + \rho\lambda^2 E\zeta\sin^2\varphi/b^2Q_h^2 \tag{21b}$$

$$a_0 = \left(1 - \rho V^2\sin^2\varphi/Q_h - R_h V^2\sin^2\varphi/\lambda Q_h\right)\bar{k}^4 + \left(\rho\lambda^2 E\zeta\sin^2\varphi/b^2Q_h^2 - \beta\rho\lambda P_h\dot{\gamma}_h V^2\sin^2\varphi/cQ_h^2\right)\bar{k}^2 + \beta\rho\lambda^3 P_h\dot{\gamma}_h E\zeta\sin^2\varphi/cb^2Q_h^3 \tag{21c}$$

$$b_1 = 2\left[(1 + R_h/\rho\lambda)\bar{k}^2 + \beta\lambda P_h\dot{\gamma}_h/cQ_h\right] \tag{21d}$$

$$b_0 = \left(1 + R_h\bar{k}^2/\rho\lambda - \beta\tau_h P_h/\rho cQ_h - \rho V^2\sin^2\varphi/Q_h\right)\bar{k}^2 + \rho\lambda^2 E\zeta\sin^2\varphi/b^2Q_h^2 \tag{21e}$$

Here, $\bar{\alpha} = \rho\lambda\alpha/Q_h$, $\bar{k} = \sqrt{\rho/Q_h}\lambda k$, $Q_h = (\partial\tau/\partial\gamma)_h$, $R_h = (\partial\tau/\partial\dot{\gamma})_h$, $P_h = -(\partial\tau/\partial\theta)_h$. Q_h, R_h, pH reflect the effect of strain hardening, strain rate hardening and thermal softening, respectively.

The question of the stability of the linearized problem becomes essentially algebraic in nature; we investigate the signs of the real part of the roots of spectral Eq. (20). To satisfy Eq. (20), it is necessary that the sum of both the imaginary part and the real part are equal to zero. According to the Routh–Hurwitz stability criterion (Sanchez, 1968), the spectral Eq. (20) can have roots with positive real parts if and only if

$$\frac{\beta\tau_h P_h}{\rho cQ_h} + \frac{\rho V^2\sin^2\varphi}{Q_h} - \left(\frac{R_h}{\rho\lambda}\bar{k}^2 + \frac{\rho\lambda^2 E\Gamma^2}{4b^2Q_h^2}\bar{k}^{-2}\right) > 1 \tag{22}$$

where $\Gamma = 2[1 + \mu\tan(\omega - \varphi)]^{1/2}\sin\varphi$.

Once instability occurs, it must occur at a special set of wave numbers for which the system is most unstable and the perturbation grows most quickly (Bai, 1982).It is worth noting that the third term $(R_h\bar{k}^2/\rho\lambda + \rho\lambda^2 E\Gamma^2\bar{k}^{-2}/4b^2Q_h^2)$ in Eq. (20) reaches its minimum value at

$$k = k_m = \left(E\Gamma^2/4R_h\lambda b^2\right)^{1/4} \tag{23}$$

When the wave number satisfies $k = (E\Gamma^2/4R_h\lambda b^2)^{1/4}$, the deformation is most unstable. Therefore, the instability criterion can be further given by

$$D = \frac{B}{1 + Pr^{-1/2}\Phi - Da} > 1 \tag{24}$$

where

$$B = \frac{\beta\tau_h P_h}{\rho cQ_h},\quad Pr = C_\upsilon/C_\lambda,\quad \Phi = \Gamma C_L C_\upsilon/C_{SP}^2,\ Da = \rho V^2\sin^2\varphi/Q_h,$$
$$C_L = \sqrt{E/\rho},\quad C_{SP} = \sqrt{Q_h/\rho},\quad C_\lambda = \lambda/b,\quad C_\upsilon = R_h/\rho b, \tag{25}$$

Here, the variable C_L represents the elastic wave velocity caused by the unloading of the tool-chip compression, and the variables C_{SP}, C_λ and C_υ reflect, respectively, the plastic shear wave velocity, the thermal diffusion velocity and the viscous diffusion velocity.

In Eq. (24), the dimensionless number B reflects the competition between thermal softening and strain hardening. This dimensionless number was first proposed by Bai (1982) to characterize the onset of thermo-plastic shear band in simple shear. Φ is the tool compression coefficient, and, Pr is a *Prandtl* number characterizing the ratio of viscous diffusion velocity to thermal diffusion velocity. Da is an effective damage number (Johnson, 1972), which

characterizes the ratio of the energy input per unit volume to the material strain hardening.

$(1 + Pr^{-1/2}\Phi - Da)^{-1}$ is an amendment to the dimensionless number *B*. As thus, the dimensionless number *D* defined in Eq. (24) can be regarded as the ratio of the effective thermal softening effect to the strain hardening effect, where the effective thermal softening effect is influenced by the *Prandtl* number *Pr*, the tool compression coefficient Φ and the effective damage number *Da*. The instability criterion (24) indicates that when the effective thermal softening effect caused by external loading overcomes the strain hardening effect of the material itself, the chip flow transition from continuous to serrated occurs.

When the effects of tool-chip compression and material convection are ignored, the problem is reduced to the thermoplastic simple shear investigated by Bai (1982). For this condition the terms *Pr*, Φ and *Da* in Eq. (24) vanish and the instability condition $B > 1$ is derived (Bai, 1982).

The tool compression coefficient Φ reflects the competition among the effects of elastic unloading of tool-chip compression, viscous diffusion and plastic shear strain hardening. A higher Φ indicates a higher energy consumption for viscous diffusion or a more severe elastic unloading of tool-chip compression, both of which retard heat concentration. It should be noticed that Φ vanishes if tool-chip compression is ignored. This causes a lower *D* and hence promotes stability. It indicates that the tool-chip compression retards the onset of instability.

The effective damage number *Da* characterizing the ratio of the energy input per unit volume to material strain hardening promotes instability. A higher *Da* indicates a higher energy input or a weakened resistance of the material against the plastic flow, both of which facilitate the emergence of shear banding. This tendency is in accordance with the instability criterion (Eq. (24)), if other terms keep unchanged.

Besides the effective damage number *Da*, the other parameters, such as *B*, *Pr* and Φ in the Eq. (24) also contain the inertial factor ρ. It is difficult to explicitly demonstrate the role of the inertial effect on the onset of instability according to the instability criterion (Eq. (24)). As reported by Molinari (1985, 1997), Zhou et al. (2006a) and Rodríguez-Martinez et al. (2015), the inertia plays a stabilizing role on the growth or development of shear banding instability in simple shear. However, for the onset of shear instability in high speed cutting, the situation is much more complex. About how the inertial influences the onset of serrated chip flow deserves further study in our future work.

In our previous work (Ye et al., 2014), we have obtained an explicit expression of the critical cutting speed for the onset of serrated chip flow based on dimensional analysis and numerical simulations. The explicit expression could give prediction of the critical cutting speed at which the chip flow changes from continuous to serrated; however, it fails on revealing the underlying reason for the onset of serrated chip flow because the explicit expression is obtained based on finite element simulations rather than physical model. Besides, the explicit expression is applicable only in a certain range because the simulated conditions are limited. In this work, we achieved the critical condition (Eq. (24)) for the onset of serrated chip flow based on the physical equations governing the chip formation process, the underlying reason for the chip flow transition from continuous to serrated is revealed. Based on the critical condition, the onset of serrated chip flow also can be predicted.

5.2. Validation of the instability criterion

In this section, we calculate the dimensionless number *D* for different cutting conditions, and then, compare the calculated results with the experimental findings to validate the instability criterion (Eq. (24)).

To calculate the dimensionless number *D*, it needs to determine the steady-state solutions of γ_h, $\dot{\gamma}_h$, θ_h and τ_h. It is known that, the shear deformation inside the PSZ is homogenous for the continuous chip flow, which is essentially a steady-state process, and the shear banding in the serrated chip flow is a result of the instability of such homogeneous shear deformation. So, we can determine the steady-state solutions of γ_h, $\dot{\gamma}_h$, θ_h and τ_h according to the homogeneous shear deformation solutions.

For given cutting conditions and work material, the evolutions of shear strain rate, shear strain, temperature and shear stress can be determined from the homogeneous shear deformation solutions (the coupling deformation). As thus, the steady-state solutions of $\dot{\gamma}_h$, θ_h and τ_h at any loading shear strain (γ_h) can be obtained.

It should be noted that, for the homogeneous deformation occurred in continuous chip flow, the deformation is more unstable at higher strains. To investigate the stability of thermoplastic flow it only needs to judge whether instability can occur at the largest loading strain $\gamma_{\max}$. The largest loading strain for the homogeneous deformation in continuously smooth chip flow can be approximately estimated by $\gamma_{\max} = \cos\omega/2\sin\varphi\cos(\varphi - \omega)$ (Oxley, 1989). At the point $\gamma_h = \gamma_{\max}$, the corresponding $\dot{\gamma}_h$, θ_h and τ_h can be determined based on the homogeneous deformation solutions. Then, the variables in Eq. (24) are determined. In this way the dimensionless number *D* is determined, and the thermoplastic flow stability can be investigated.

Fig. 9 shows the evolution of the dimensionless number *D* with cutting speed for various materials. In this figure, the solid and hollow patterns indicate that the chips obtained from the corresponding cutting experiments are continuous and serrated, respectively. Some other published experimental data (Atlati et al., 2011; Gao et al., 2011; Joshi, 2000; Lorentzon et al., 2009; Mabrouki et al., 2008; Ng et al., 2002; Sun et al., 2009; Ye et al., 2012) are also given in this figure to validate our model. The mechanical properties and parameters for the work materials involved in Fig. 7 (Copper, Al 2025, Al 7075, AISI 1045, AISI 4340, IN 718, Ti-6Al-4 V) are given in Table 6 (Atlati et al., 2011; Brar et al., 2009; Fang and Zeng, 2007; Hussain et al., 2013; Jaspers and Dautzenberg, 2002; Lee and Lin, 1998; Pereira and Lerch, 2001).

Fig. 9 shows that the numerical calculation results for the dimensionless number *D* agree with the experimental findings; only a few data do not accord well with the experimental results. It can be seen that the flow patterns are serrated in the zone of $D > 1$ and that the continuous flow patterns fall in the zone of $D < 1$. Most importantly, the transition of the flow pattern from continuous to serrated almost always occurs around $D = 1$. In Fig. 9, the materials involved are copper, aluminium alloys, steels, titanium alloy and nickel-base superalloy, which are the most typical metallic work materials. This figure implies that the instability criterion (24) allows the prediction of the transition of chip flow from continuous to serrated.

6. Scaling law of serration frequency

When the cutting speed is increased to a certain critical value, thermo-mechanical deformation in the PSZ meets the instability condition; therefore, shear banding forms in the PSZ. The shear banding initiation and propagation will decrease the shear stress because of energy dissipation. Consequently, heat production is reduced, and the PSZ is cooled by diffusion and material convection. Soon, however, as the tool continues moving, new uncut material passes through the PSZ for another build-up in stress and temperature. This cutting cycle repeats itself, and a serrated flow forms.

Once the serrated flow forms, the flow motion becomes periodic; it is composed of regularly distributed shear bands. The spac-

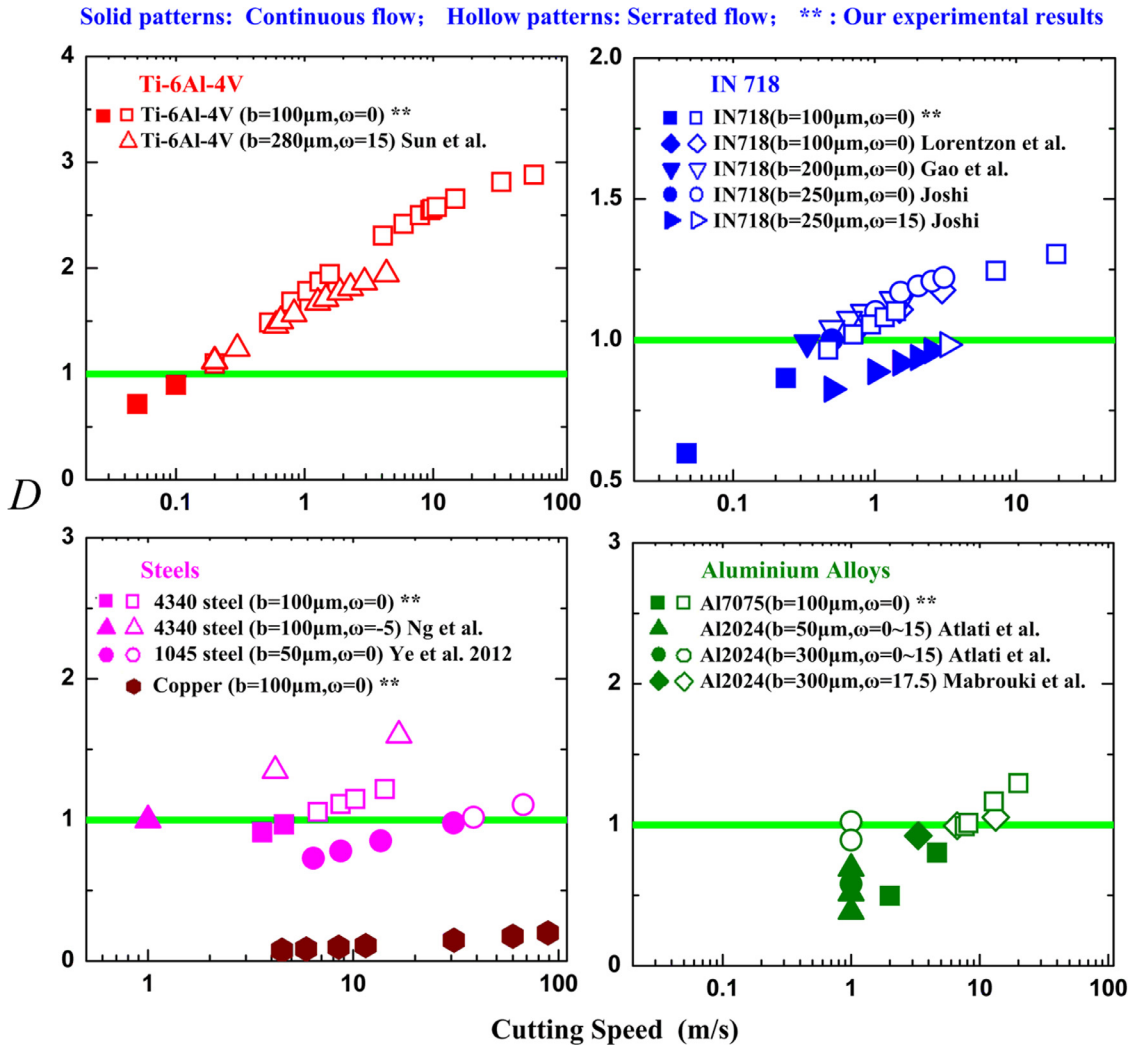

Fig. 9. Evolution of the dimensionless number Das function of cutting speed.

Table 6
Mechanical properties and parameters.

Properties and parameters	C10200	Al 2024	Al7075	AISI 1045	AISI4340	Ti-6Al-4V	IN718
Elastic Modulus (E) GPa	129	73	71	205	200	105	210
Density (ρ) kg m^{-3}	8960	2700	2770	7800	7860	4430	8200
Thermal diffusivity (λ) $\times 10^{-6}$ m^2 s^{-1}	116	46	53	12	13	3	3
Specific heat (c) J kg^{-1} K^{-1}	383	400	885	420	473	520	435
Initial yield stress (τ_A) MPa	58	203	315	319	457	452	780
Hardening modulus (τ_B) MPa	169	254	391	346	294	287	657
Strain rate coefficient (C)	0.025	0.0083	0.024	0.0134	0.014	0.028	0.014
Work-hardening exponent (n)	0.31	0.42	0.71	0.234	0.26	0.28	0.65
Thermal softening exponent (m)	1.09	1	1.56	1	1.03	1.00	1.00
The reference stain rate ($\dot{\gamma}_{ref}$) s^{-1}	1.73	1.73	1.73	1.73	1.73	1.73×10^{-5}	1.73
Melting temperature (θ_{melt}) K	1356	768	893	1733	1793	1880	1570

ing of these regularly spaced shear bands, i.e., the serration spacing, is related to the characteristic perturbation wave number for which the corresponding perturbation growth rate could achieve a peak maximum value (Bai, 1982; Wright, 2002). From the stability analysis, we have determined that when the wave number k_m satisfies $k_m = (E\Gamma^2/4R_h\lambda b^2)^{1/4}$ (see Eq.(23)), the perturbation grows most quickly. The corresponding segment spacing L_c can be obtained as $L_c = 2\pi/k_m$ (Wright, 2002), that is,

$$L_c = 2\pi/k_m = \Lambda \cdot \left(\frac{R_h\dot{\gamma}\lambda b^3}{\Omega E}\right)^{1/4} \cdot V^{-1/4} \tag{26}$$

where $\Omega = b/w$, and Λ is defined as $\Lambda = 2\pi[4\cos(\omega-\varphi)/(\Gamma^2\cos\omega)]^{1/4}$.

Based on Eq. (26), the chip serration frequency f can be given by

$$f = \frac{V_f}{L_c} = \Lambda^{-1}\sin\varphi \cdot \left(\frac{\Omega E}{R_h\dot{\gamma}\lambda b^3}\right)^{1/4} V^{5/4} \tag{27}$$

For most metallic materials, there is a linear proportion by inversion between R_h and shear strain rate, so $R_h\dot{\gamma}$ can be regarded as speed-independent (Molinari et al., 2002). Moreover, the shear angle is weakly dependent on V (Molinari et al., 2002). Thus,

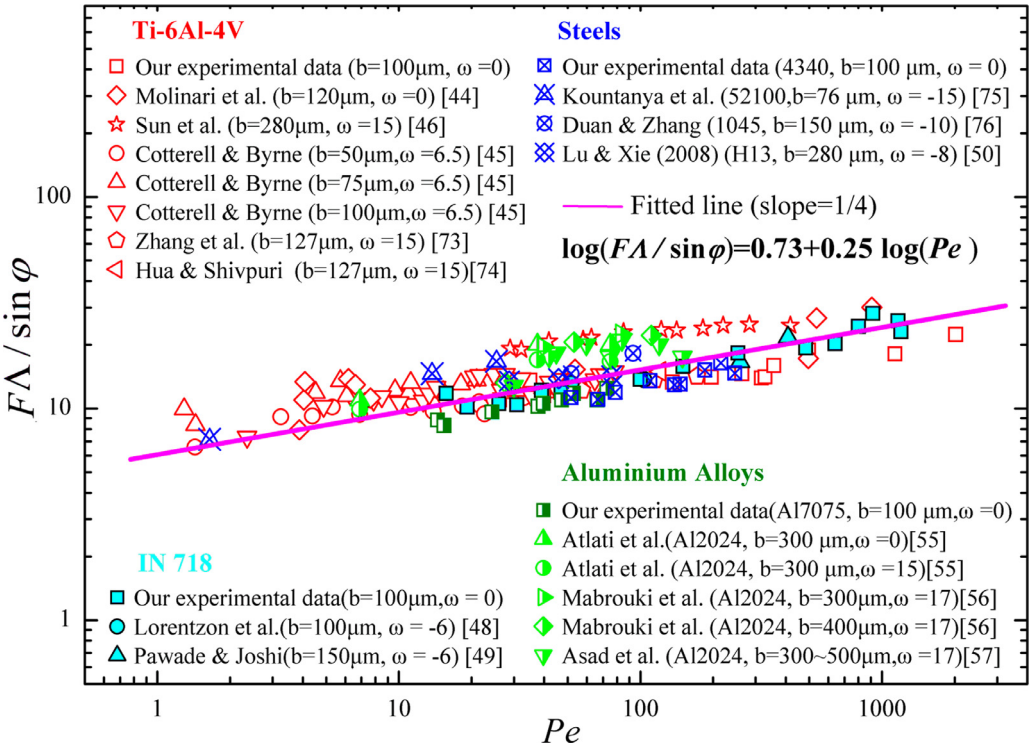

Fig. 10. $F\Lambda/\sin\varphi$ plotted with Pe for various materials.

Eq. (27) indicates that the serration frequency f follows a power scaling law as a function of cutting speed according to $f \propto V^{5/4}$, which matches well with the experimental results; see Figs. 4 and 5.

It is worth noting that by modelling the thermo-plastic deformation that occurs in high-speed cutting to a simple shear, Molinari et al., (2002; 2013) discovered a 7/4 power law relation for serration frequency through perturbation analysis. Here, with considering the complex loading conditions in HSM, a 5/4 scaling law is achieved for serration frequency. It should be noted that in the case of HSM, large-scale shearing deformation inside the PSZ is caused by the tool-chip compression (Burns and Davies, 2002), the unloading of which reduces the energy input into the PSZ. In addition, in the case of HSM, the rapid chip flow takes heat away from the PSZ by means of material convection. Both the tool-chip compression unloading and material convection become more severe at higher cutting speeds. Thus, in comparison to simple shear, more energy can be consumed in HSM, and less energy needs to be dissipated by shear banding. In this way, fewer additional shear bands should form in the serrated chip flow with increasing loading velocity, indicating a more slowly increasing shear band frequency.

Rearranging, and using variables $F = fb/V$ and $Pe = Vb/\lambda$, Eq. (27) is rewritten as:

$$F = \Lambda^{-1} \sin\varphi \cdot [E\Omega/(R_h\dot{\gamma})]^{1/4} \cdot Pe^{1/4} \tag{28}$$

Here, F is a *Deborah* number (Reiner, 1964), which reflects the ratio of the time for external loading to the time for each serration formation. *Pe* is a *Péclect* number, representing the ratio of transit time to relaxation time. In metal cutting, *Pe* is also called the *Reynolds* thermal number (Bisacre and Bisacre, 1947) or thermal number (Childs, 2013). It was first introduced by Bisacre and Bisacre (1947) to study the tool-life problem. The serrated chip flow usually occurs when *Pe* is large (Childs, 2013; Drucker and Ekstein, 1950).

Eq. (28) indicates that F follows a power-law dependence on Pe: $F \propto Pe^{1/4}$. In Fig. 10, to eliminate the tool rake angle effect, $F\Lambda/\sin\varphi$ is plotted as a function of *Pe* on a double logarithmic scale. This figure is derived from data presented by various authors (Asad et al., 2008; Atlati et al., 2011; Cotterell and Byrne, 2008; Duan and Zhang, 2012; Hua and Shivpuri, 2004; Kountanya et al., 2009; Lorentzon et al., 2009; Lu and Xie, 2008; Mabrouki et al., 2008; Molinari et al., 2002; Pawade and Joshi, 2011; Sun et al., 2009; Zhang et al., 2011). All of the data for Ti-6Al-4V, IN 718, aluminium alloys and steels can be fitted by a universal straight line with a slope of 1/4. Varying cutting speeds from 0.01 to 63 m/s and uncut chip thicknesses from 50 to 500 μm lead to a change in *Pe* over 4 orders of magnitude. Fig. 10 nevertheless shows that, even over this wide parameter space, a universal dependence is still obtained.

7. Conclusions

In conclusion, systematic HSM experiments have shown that the serrated chip flow can be attributed to repeated catastrophic thermoplastic shear instability occurring in the PSZ. Based on the experimental observation, a high-speed cutting model that takes into consideration inertial effect, material convection and tool-chip compression was developed. The basic equations governing the thermo-mechanical flow inside the PSZ were also established. We have further achieved the initiation condition for serrated chip flow by using the perturbation analysis method. It is demonstrated that the continuous-serrated transition of chip flow is controlled by a dimensionless number D which reflects the competition between effective thermal softening and strain hardening. After a periodically serrated chip flow forms, there exists a scaling law between its frequency and the *Reynolds* thermal number *Pe*. All of these facts provide new insight into the nature of the chip flow instability in HSM.

Acknowledgements

Financial support is from NSFC (Grants nos. 11472287, 11132011, 11402278, 11572324, 11372315, 11522221), the Key Researh Program of Frontier Sciences (Grant No. QYZDJSSW-JSC011), the Strategic Priority Research Program of the Chinese Academy of Sciences (Grant No. XDB22040302) and the Fundamental Research Funds for the Central Universities (Grant No. 15CX02110A).

References

Aifantis, E.C., 1987. The physics of plastic deformation. Int. J. Plast. 3, 211–247.
Asad, M., Girardin, F., Mabrouki, T., Rigal, J.F., 2008. Dry cutting study of an aluminium alloy (A2024-T351): a numerical and experimental approach. Int. J. Mater. Form. Suppl 1, 499–502.
Atkins, A.G., 2009. The Science and Engineering of Cutting. Elsevier, Oxford.
Atlati, S., Haddag, B., Nouari, M., Zenasni, M., 2011. Analysis of a new Segmentation Intensity Ratio "SIR" to characterize the chip segmentation process in machining ductile metals. Int. J. Mach. Tool. Manuf. 51, 687–700.
Bai, Y.L., 1982. Thermo-plastic instability in simple shear. J. Mech. Phys. Solids 30, 195–207.
Bai, Y.L., Dodd, B., 1992. Adiabatic Shear Localization. Pergamon Press, Oxford.
Batra, B.C., 1987. The initiation and growth of, and the interaction among adiabatic shear bands in simple and dipolar materials. Int. J. Plast. 3, 75–89.
Batra, R.C., Kim, C.H., 1990. Effect of viscoplastic flow rules on the initiation and growth of shear bands at high strain rates. J. Mech. Phys. Solids 38, 859–874.
Batra, R.C., Wei, Z.G., 2006. Shear band spacing in thermoviscoplastic materials. Int. J. Impact. Eng. 32, 947–967.
Bisacre, F.F.P., Bisacre, G.H., 1947. The life of carbide-tipped turning tools. Pro I Mech Eng 157, 452–469.
Brar, N.S., Joshi, V.S., Harris, B.W., 2009. Constitutive model constants for Al 7075-T651 and Al7075-T6. In: Elert, M., Furnish, M.D., Anderson, W.W., Proud, W.G., Butler, W.T. (Eds.), AIP Conf. Proc., American Institute of Physics. Nashville, pp. 945–948.
Burns, T.J., Davies, M.A., 1997. Nonlinear dynamics model for chip segmentation in machining. Phys. Rev. Lett. 79, 447–450.
Burns, T.J., Davies, M.A., 2002. On repeated adiabatic shear band formation during high-speed machining. Int. J. Plast. 18, 487–506.
Cai, S.L., Chen, Y., Ye, G.G., Jiang, M.Q., Wang, H.Y., Dai, L.H., 2015. Characterization of the deformation field in large-strain extrusion machining. J. Mater. Process. Technol. 216, 48–58.
Cai, S.L., Dai, L.H., 2014. Suppression of repeated adiabatic shear banding by dynamic large strain extrusion machining. J. Mech. Phys. Solids 73, 84–102.
Calamaz, M., Coupard, D., Girot, F., 2010. Numerical simulation of titanium alloy dry machining with a strain softening constitutive law. Mach. Sci. Technol. 14, 244–257.
Campbell, C., Bendersky, L., Boettinger, W., Ivester, R., 2006. Microstructural characterization of Al-7075-T651 chips and work pieces produced by high-speed machining. Materials Science and Engineering: A 430, 15–26.
Childs, T.H.C., 2013. Adiabatic shearing in metal machining. In: Laperrière, L., Reinhart, G. (Eds.), CIRP Encyclopaedia of Production Engineering, Eds.. Springer, Berlin.
Cotterell, M., Byrne, G., 2008. Dynamics of chip formation during orthogonal cutting of titanium alloy Ti-6Al-4V. CIRP Ann.-Manuf. Techn. 57, 93–96.
Daridon, L., Oussouaddi, O., Ahzi, S., 2004. Influence of the material constitutive models on the adiabatic shear band spacing: MTS, power law and Johnson–Cook models. Int. J. Solids. Struct. 41, 3109–3124.
Dodd, B., Bai, Y.L., 2012. Adiabatic Shear Localization, 2nd ed Elsevier, London.
Dodd, B., Bai, Y.L., 2014. An Introduction to Adiabatic Shear. Imperial College Press, London.
Dodd, B., Walley, S.M., Yang, R., Nesterenko, V.F., 2015. Major steps in the discovery of adiabatic shear bands. Metall. Mater. Trans. 46, 4454–4458.
Drucker, D.C., Ekstein, H., 1950. A dimension analysis of metal cutting. J. Appl. Phys. 21, 104–107.
Duan, C.Z., Wang, M.J., 2004. Adiabatic shear bands in 30CrNi3MoV structural steel induced during high speed cutting. J. Mater. Sci. Tech. 20.
Duan, C.Z., Zhang, L.C., 2012. Adiabatic shear banding in AISI 1045 steel during high speed machining: mechanisms of microstructural evolution. Mater. Sci. Eng. A 532, 111–119.
Fang, G., Zeng, P., 2007. FEM investigation for orthogonal cutting process with grooved tools–technical communication. Mach. Sci. Technol. 11, 561–572.
Gao, D., Hao, Z., Han, R., Chang, Y., Muguthu, J.N., 2011. Study of cutting deformation in machining nickel-based alloy Inconel 718. Int. J. Mach. Tool. Manuf. 51, 520–527.
Grady, D.E., 1994. Dissipation in adiabatic shear bands. Mech. Mater. 17, 289–293.
Grady, D.E., Olsen, M.L., 2003. A statistics and energy based theory of dynamic fragmentation. Int. J. Impact. Eng. 29, 293–306.
Hou, Z.B., Komanduri, R., 1997. Modelling of thermomechanical shear instability in machining. Int. J. Mech. Sci. 39, 1279–1314.
Hua, J., Shivpuri, R., 2004. Prediction of chip morphology and segmentation during the machining of titanium alloys. J. Mater. Process. Technol. 150, 124–133.
Huang, J., Aifantis, E.C., 1997. A note on the problem of shear localization during chip formation in orthogonal machining. J. Mater. Eng. Perform. 6, 25–26.
Huang, J., Kalaitzidou, K., Sutherland, J.W., Aifantis, E.C., 2007. Validation of a predictive model for adiabatic shear band formation in chips produced via orthogonal machining. J. Mech. Behav. Mater. 18, 243–263.
Hussain, G., Hameed, A., Hetherington, J.G., Barton, P.C., Malik, A.Q., 2013. Hydrocode simulation with modified Johnson–Cook model and experimental analysis of explosively formed projectiles (copper). J. Energ. Mater. 31, 143–155.
Jaspers, S.P.F.C., Dautzenberg, J.H., 2002. Material behaviour in conditions similar to metalcutting: flow stress in the primary shear zone. J. Mater. Process. Technol. 122, 322–330.
Johnson, W., 1972. Impact Strength of Materials. Edward Arnold, London.
Joshi, D., 2000. Finite element simulation of machining a Nickel-based superalloy - Inconel 718, University of Pune. University of Pune, India.
Kountanya, R., Al-Zkeri, I., Altan, T., 2009. Effect of tool edge geometry and cutting conditions on experimental and simulated chip morphology in orthogonal hard turning of 100Cr6 steel. J. Mater. Process. Technol. 209, 5068–5076.
Lee, W.S., Lin, C.F., 1998. High-temperature deformation behaviour of Ti6Al4V alloy evaluated by high strain-rate compression tests. J. Mater. Process. Technol. 75, 127–136.
Lorentzon, J., Järvstråt, N., Josefson, B.L., 2009. Modelling chip formation of alloy 718. J. Mater. Process. Technol. 209, 4645–4653.
Love, B.M., Batra, R.C., 2010. Effect of particulate/matrix debonding on the formation of adiabatic shear bands. Int. J. Mech. Sci. 52, 386–397.
Lu, S.H., Xie, Q.Y., 2008. Study on adiabatic shear behaviour in orthogonal cutting of H13 steel. In: Yan, X.T., Jiang, C.Y., Eynard, B. (Eds.), Advanced Design and Manufacture to Gain a Competitive Edge. Springer, London, pp. 189–198.
Mabrouki, T., Girardin, F., Asad, M., Rigal, J.F., 2008. Numerical and experimental study of dry cutting for an aeronautic aluminium alloy (A2024-T351). Int. J. Mach. Tool. Manuf. 48, 1187–1197.
Mallock, A., 1881. The action of cutting tools. Proc. R. Soc. Lond. 33, 127–139.
Meyers, M.A., 1994. Dynamic Behavior of Materials. Wiley, New York.
Molinari, A., 1985. Thermo-visco plastic in stability in simple shear. J.Theor.Appl.Mech. 4, 659–684.
Molinari, A., 1997. Collective behavior and spacing of adiabatic shear bands. J. Mech. Phys. Solids 45, 1551–1575.
Molinari, A., Dudzinski, D., 1992. Stationary shear band in high-speed machining. CR. Acad. Sci. Paris 315, 399–405.
Molinari, A., Musqua, C., Sutter, G., 2002. Adiabatic shear banding in high speedmachining of Ti-6Al-4V: experiments and modelling. Int. J. Plast. 18, 443–459.
Molinari, A., Soldani, X., Miguélez, M.H., 2013. Adiabatic shear banding and scaling laws in chip formation with application to cutting of Ti-6Al-4V. J. Mech. Phys. Solids 61, 2331–2359.
Nemat-Nasser, S., Guo, W.-G., 2003. Thermomechanical response of DH-36 structural steel over a wide range of strain rates and temperatures. Mech. Mater. 35, 1023–1047.
Nemat-Nasser, S., Guo, W.-G., 2005. Thermomechanical response of HSLA-65 steel plates: experiments and modelling. Mech. Mater. 37, 379–405.
Nemat-Nasser, S., Guo, W.G., Nesterenko, V.F., Indrakanti, S.S., Gu, Y.B., 2001. Dynamic response of conventional and hot isostatically pressed Ti–6Al–4V alloys: experiments and modelling. Mech. Mater. 33, 425–439.
Nemat-Nasser, S., Okada, N., 2001. Radiographic and microscopic observation of shear bands in granular materials. Geotechnique 51, 753–765.
Ng, E.-G., El-Wardany, T.I., Dumitrescu, M., Elbestawi, M.A., 2002. Physics-based simulation of high speed machining. Mach. Sci. Technol. 6, 301–329.
Osovski, S., Rittel, D., Venkert, A., 2013. The respective influence of microstructural and thermal softening on adiabatic shear localization. Mech. Mater. 56, 11–22.
Oxley, P.L.B., 1989. Mechanics of Machining. Wiley, New York.
Pawade, R.S., Joshi, S.S., 2011. Mechanism of chip formation in high-speed turning of Inconel 718. Mach. Sci. Technol. 15, 132–152.
Pereira, J.M., Lerch, B.A., 2001. Effects of heat treatment on the ballistic impact properties of Inconel 718 for jet engine fan containment applications. Int. J. Impact. Eng. 25, 715–733.
Ramesh, K.T., 1994. On the localization of shearing deformations in a tungsten heavy alloy. Mech. Mater. 17, 165–173.
Recht, R.F., 1964. Catastrophic theroplastic shear. J. Appl. Mech. 189–193.
Reiner, M., 1964. The Deborah number. Phys. Today 17, 62.
Rittel, D., 1998. The influence of temperature on dynamic failure mode transitions. Mech. Mater. 30, 217–227.
Rittel, D., Landau, P., Venkert, A., 2008. Dynamic recrystallization as a potential cause for adiabatic shear failure. Phys. Rev. Lett. 101, 165501.
Rittel, D., Wang, Z., Merzer, M., 2006. Adiabatic shear failure and dynamic stored energy of cold work. Phys. Rev. Lett. 96, 075502.
Rittel, D., Wang, Z.G., 2008. Thermo-mechanical aspects of adiabatic shear failure of AM50 and Ti6Al4V alloys. Mech. Mater. 40, 629–635.
Rodríguez-Martínez, J.A., Vadillo, G., Rittel, D., Zaera, R., Fernández-Sáez, J., 2015. Dynamic recrystallization and adiabatic shear localization. Mech. Mater. 81, 41–55.
Sanchez, D.A., 1968. Ordinary Differential Equations and Stability Theory. Freeman, San Francisco.
Semiatin, S.L., Rao, S.B., 1983. Shear localization during metal-cutting. Mater. Sci. Eng. A 61, 185–192.
Shaw, M.C., 2005. Metal Cutting Principles, 2nd ed Oxford University Press, New York.
Su, S., Stainier, L., 2015. Energy-based variational modelling of adiabatic shear bands structure evolution. Mech. Mater. 80, 219–233.

Sun, S., Brandt, M., Dargusch, M.S., 2009. Characteristics of cutting forces and chip formation in machining of titanium alloys. Int. J. Mach. Tool. Manuf. 49, 561–568.
Sutter, G., Faure, L., Molinari, A., Delime, A., Dudzinski, D., 1997. Experimental analysis of the cutting process and chip formation at high speed machining. J. Phys. IV France 07, 33–38.
Sutter, G., List, G., 2013. Very high speed cutting of Ti–6Al–4V titanium alloy – change in morphology and mechanism of chip formation. Int. J. Mach. Tool. Manuf. 66, 37–43.
Tresca, H., 1878. On further application of the flow of solids. Pro. Inst. Mech. Eng. 301.
Tvergaard, V., 2015. Effect of initial void shape on ductile failure in a shear field. Mech. Mater. 90, 2–9.
Vyas, A., Shaw, M.C., 1999. Mechanics of saw-tooth chip formation in metal cutting. J. Manuf. Sci. Eng. 121, 163–172.
Walley, S.M., 2007. Shear localization: a historical overview. Metall. Mate. Trans. A 38, 2629–2654.
Wright, T.W., 2002. The Physics and Mathematics of Adiabatic Shear Bands. Cambridge university press, Cambridge.
Wu, X.Y., Ramesh, K.T., Wright, T.W., 2003. The dynamic growth of a single void in a viscoplastic material under transient hydrostatic loading. J. Mech. Phys. Solids 51, 1–26.
Xue, Q., Meyers, M.A., Nesterenko, V.F., 2002. Self-organization of shear bands in titanium and Ti-6Al-4V alloy. Acta Mater. 50, 575–596.
Yang, Q., Liu, Z., Wang, B., 2012. Characterization of chip formation during machining 1045 steel. Int. J. Adv. Manuf. Tech 63, 881–886.
Ye, G.G., Chen, Y., Xue, S.F., Dai, L.H., 2014. Critical cutting speed for onset of serrated chip flow in high speed machining. Int. J. Mach. Tool. Manuf. 86, 18–33.
Ye, G.G., Xue, S.F., Ma, W., Jiang, M.Q., Ling, Z., Tong, X.H., Dai, L.H., 2012. Cutting AISI 1045 steel at very high speeds. Int. J. Mach. Tool. Manuf. 56, 1–9.
Yuan, F., Bian, X., Jiang, P., Yang, M., Wu, X., 2015. Dynamic shear response and evolution mechanisms of adiabatic shear band in an ultrafine-grained austenite—ferrite duplex steel. Mech. Mater. 89, 47–58.
Zhang, H., Jing, X., Subhash, G., Kecskes, L.J., Dowding, R.J., 2005. Investigation of shear band evolution in amorphous alloys beneath a Vickers indentation. Acta Mater 53, 3849–3859.
Zhang, H., Maiti, S., Subhash, G., 2008. Evolution of shear bands in bulk metallic glasses under dynamic loading. J. Mech. Phys. Solids 56, 2171–2187.
Zhang, Y.C., Mabrouki, T., Nelias, D., Gong, Y.D., 2011. Chip formation in orthogonal cutting considering interface limiting shear stress and damage evolution based on fracture energy approach. Finite. Elem. Anal. Des. 47, 850–863.
Zhou, F., Molinari, J.F., Ramesh, K.T., 2006a. An elastic–visco-plastic analysis of ductile expanding ring. Int. J. Impact. Eng. 33, 880–891.
Zhou, F., Wright, T., Ramesh, K., 2006b. The formation of multiple adiabatic shear bands. J. Mech. Phys. Solids 54, 1376–1400.
Zhou, M., Ravichandran, G., Rosakis, A.J., 1996. Dynamically propagating shear bands in impact-loaded prenotched plates-I and II. J. Mech. Phys. Solids 44, 1023–1032 981-1021.